Title
DEVELOPMENT OF THE HELIUM-JET FED ON-LINE MASS SEPARATOR RAMA, I

Author
Moltz, D.M.

Publication Date
1979-12-01

LBL-9476 c.2
Preprint

Lawrence Berkeley Laboratory
UNIVERSITY OF CALIFORNIA

Submitted to Nuclear Instruments and Methods

DEVELOPMENT OF THE HELIUM-JET FED ON-LINE MASS SEPARATOR RAMA, I

D. M. Moltz, R. A. Gough, M. S. Zisman, D. J. Vieira, H. C. Evans, and J. Cerny

December 1979

Prepared for the U.S. Department of Energy under Contract W-7405-ENG-48

DEVELOPMENT OF THE HELIUM-JET FED ON-LINE MASS SEPARATOR RAMA, I*

D. M. Moltz, R. A. Gough, M. S. Zisman, D. J. Vieira**
H. C. Evans†, and Joseph Cerny

Department of Chemistry and
Lawrence Berkeley Laboratory
University of California
Berkeley, California 94720

December 1979

ABSTRACT

Development of general experimental systems capable of mass analysis of radioactive species with half-lives as short as 50 ms and with simple application to a vast majority of the chemical elements is clearly of great interest in the study of nuclei far from stability. Such an on-line system has been developed which employs a helium-jet to transport activity from the target area to a mass separator. The initial development and early experimental use of this recoil atom mass analysis system (RAMA) are described. RAMA has a typical total efficiency of 0.01%, which should apply to ~75 elements of melting point <2000°C. This efficiency is for a mass resolution $M/\Delta M \sim 200$.

* This work was supported by the Nuclear Physics and Nuclear Sciences Divisions of the U. S. Department of Energy under contract No. W-7405-ENG-48.

**Present Address: Los Alamos Scientific Laboratory, Los Alamos, New Mexico 87545

†Permanent Address: Physics Department, Queen's University, Kingston, Ontario, Canada.

1. Introduction

Decay studies of both neutron deficient and neutron rich nuclei become increasingly difficult the further one explores from the line of β-stability. Conventional experimental techniques often are inadequate because competing reactions create a formidable background interfering with the study of nuclei with low production cross sections. Ideally, one would like to develop a technique which would yield a sample with a unique A and Z. Z identification has long been accomplished by chemical separations, but even with the advent of some fast chemistry techniques[1,2], the study of activities with half-lives below 1 s generally remains impossible. Chemical techniques yield no mass identification, however, leading to experiments which establish parent-daughter relationships in which the daughter has been previously characterized. Most compound nuclear reactions produce many isobars simultaneously, making mass separation very necessary.

Since most of the undiscovered nuclides are expected to have half-lives too short for off-line techniques, on-line mass analysis is a highly suitable approach for studying their decays. Many ingenious approaches to the development of such techniques have been tried. Isotope separator on-line (ISOL) systems have been developed to utilize many different accelerators and reactors.[3-12]

At the LBL 88-Inch Cyclotron, we were interested in developing an ISOL system capable of studying radioactive species with half-lives as short as 50 ms and with simple application to most of the chemical elements. Experiments of immediate concern were the study of the

decay of the A = 4n, T_z = -2, series of nuclei since, in general, these nuclei decay via β-delayed proton emission permitting accurate measurement of the lowest T = 2 state in the T_z = -1 member of an isospin quintet. Complete isospin quintets would permit further testing of the isobaric multiplet mass equation (IMME) first proposed by Wigner[13] and tested extensively in isobaric quartets.[14] Another area of interest is the study of nuclei near the Z = 50 closed shell. These nuclei exhibit beta-delayed particle emission and alpha-particle decay in addition to standard β-γ decay. Work in this region has already been started on a major scale at GSI[8], with the goal being the possible observation of $^{100}_{50}$Sn, a second doubly closed shell tin isotope. An excellent review of ISOL systems has been prepared by Hansen.[15]

Below we wish to describe the new Berkeley on-line mass separator RAMA, an acronym for Recoil Atom Mass Analyzer. RAMA is shown schematically in Fig. 1. RAMA couples the helium-jet recoil transport method[16] with mass spectrometry techniques. The idea for such an ISOL system was originally proposed by Nitschke[17] and used ultrapure helium as a transport gas. For reasons that will become obvious later, ultrapure helium is not conducive to efficient transport.

2. RAMA

The description of RAMA may be conveniently divided into four distinct parts: the gas-jet, the ion source, the beam transport system, and the detection systems. Each of these topics will be dealt with in terms of those techniques which have been found to work well in the RAMA system. The special problems associated with coupling a gas jet to an ion source will be delineated in addition to problems arising from transport of large beam currents (~200 μA). These four components may be tied together by considering what happens to a sample nucleus of interest. This radioactive nucleus is produced in a bombardment, recoils from the target (see Fig. 1), stops in the helium in which it attaches to an aerosol, and is subsequently swept through the 6 m long capillary tube away from the region of high background. After exiting the capillary tube with approximately sonic velocity, this aerosol passes through a 1.4 mm skimmer designed to eliminate most of the accompanying helium. Then the aerosol enters the ion source where it is broken up and the radioactive atom is ionized to the +1 oxidation state in a gas-supported arc discharge plasma. The ion of interest is extracted from the ion source by a 10.5 kV potential. This 10.5 keV particle is then transported through the optics system and collected on the focal plane for decay studies.

2.1 Helium-Jet

The gas-jet recoil transport method has been studied extensively using several carrier gases with many different additives.[18-21] No

attempt will be made here to review comprehensively all of the helium-jet methods, only to give details of the technique which has been proven to work for the RAMA system. The helium-jet requires additives[19,21] for efficient transport; successful transport of activity has been obtained using acetone, carbon tetrachloride, benzene, methanol, water, ethylene glycol, mechanical pump oil, sodium chloride, and in some cases, small amounts of air.

It is now known that these additivies or impurities form large molecular weight clusters or aerosols ranging in size from 10^3-10^8 AMU.[22] In the RAMA system formation of these aerosols requires a sufficient quantity of ionizing radiation[19,23] created by passage of the cyclotron beam through the helium. An adequate level of radiation is provided by ~1 μA of 40 MeV protons. This beam intensity requirement has been observed to scale roughly as $(dE/dx)^{-1}$ for heavier projectiles (i.e., heavier projectiles have a larger dE/dx and thus less beam intensity is required for adequate cluster formation).

An additional constraint is placed upon the RAMA helium-jet which is unimportant for most systems. Geometrical considerations for coupling the helium-jet to an ion source dictate that most of the clusters exit the capillary tube in a small forward cone (~2^o opening angle).[24] This requirement for the exiting clusters necessitates that the aerosols be very massive, 10^6-10^8 AMU. We have found that three of the additives mentioned above appear best to meet this criterion: ethylene glycol, mechanical pump oil, and sodium chloride. The last works well, but extreme care must be taken in

heating the sodium chloride beyond ~550-600°C, or excess quantities of sodium chloride will tend to clog the capillary tube. Both of the other additives work well, but ethylene glycol has traditionally been used in our experiments because its vapor pressure curve exhibits large vapor pressure changes with small temperature variations in the room temperature region. This allows us to control its concentration more easily.

Figure 2 is a photograph of the helium-jet target box.[25] The water cooled entrance and exit windows are constructed of 2.29 μm pinhole-free Havar[26] foil and isolate the 1.3 atm of He from the cyclotron and Faraday cup vacuum systems. The target (shown in Fig. 1) is mounted on a movable target wheel directly in front of the copper collection cylinder. A separate set of degrader foils may be placed in front of the target to vary the bombarding energy. Nuclear reaction products recoil out of the target in a forward cone, and are thermalized in the helium. They attach to the high molecular weight clusters and are then drawn toward the capillary opening (on the far side in Fig. 2) and transported away from the region of high background through the 1.0 mm ID, 6 m long capillary tube. The total transit time is ~200 ms. (More discussion of transit time may be found in the following paper.[27])

Several perturbations may affect transport of these clusters through the capillary tube. Generally, the helium is entrained in a laminar flow with the interactions of the helium atoms serving to concentrate the heavy clusters in the center of the flow pattern.[28]

These collisions accelerate the clusters until their axial velocity approaches that of the helium atoms. Upon exiting the capillary tube, these heavy clusters have attained sonic velocity ($\sim 10^5$ cm s^{-1}) and thus considerable energy and momentum (relative to thermal molecules). Perturbations to this laminar flow which could either partially or completely eliminate transport include blockages and charge buildup. Blockages are the most detrimental to efficient transport, with tubing kinks and particulate blockages (e.g., ethylene glycol droplets or sodium chloride crystals) being the principal offenders. Charge buildup might be a problem associated with the use of capillary tubes constructed from insulating materials and is avoided in the RAMA system by using annealed stainless steel tubing.

Sonic expansion of a perfect gas expanding isentropically into a vacuum may be treated either as a spherically symmetric flow or as a cylindrically symmetric flow. For the latter, the shape of the gas jet becomes an elliptic paraboloid, and this leads to the simple relationship[29]

$$\frac{F_z}{F_o} = \frac{s}{B_1 z} \tag{1}$$

where F_z is the gas flow rate through a skimmer at a distance z and F_o is the flow rate at the exit of the capillary tube. B_1 is a constant dependent only upon the nature of the gas (B_1 is very large for light masses), and s is the skimmer hole cross sectional area.

Simple experiments[29] have shown that Equation(1) holds for our helium-jet operating conditions in which we used a 1 cm axial distance for the skimmer (1.4 mm orifice) and employed a 1 mm ID capillary tube. Now if we consider each cluster molecule as an individual entity with no cluster-cluster interactions (the ratio of helium atoms to clusters is 10^{11} - 10^{14}), the clusters can be treated like a very heavy ideal gas. The mass dependent B_1 values (see equation (1)) for both helium and the clusters are very different, with B_1 for the clusters being very small. This shows why most of the helium strikes the skimmer and is pumped away while most of the clusters pass through the skimmer undeflected.

Shockwave effects must also be considered in the design of a skimmer.[29] Particles exiting a nozzle with sonic velocity create a shock wave which may be reflected from a solid object, and thus, some interference would be expected. A conical shape for the skimmer was originally explored to minimize the effects of this shock wave. Our results concur with those of Schmeing, et al.[30] and indicate that no appreciable differences exist between conical and flat skimmers. This result is most easily rationalized in terms of the large energy and momentum of each cluster in relation to shockwave distortions in the vicinity of the skimmer orifice.

Use of ethylene glycol with sufficient beam intensities to create clusters generally gives good total transport efficiency; however, the skimmer efficiency varies appreciably. More reproducibility was observed when cold nitrogen gas-cooled entrance and exit foils were

added to increase the beam intensity which could be tolerated on target. These initial helium-jet inconsistencies were tolerable in RAMA only in the study of high-yield reactions. More details of later improvements developed to increase system reliability are given in the following paper.[27]

2.2 Ion Source

The choice of an ion source for an ISOL system is not easily made because of the great variety of sources which have been tried with varying degrees of success. (See the recent review by Sidenius.[31]) For the RAMA system, a source was desired which met the following requirements:

a) acceptable efficiency and reasonable chemical universality;

b) stable plasma and other operating conditions; and

c) short hold-up times.

(A similar set of criteria was investigated by Kirchner and Roeckl[32-34] in choosing an appropriate ion source for the GSI on-line mass separator at the UNILAC.)

The type of ion source which appeared best to fit all of these criteria and which could be coupled to the helium-jet was an early Sidenius-type hollow cathode ion source.[35] A schematic diagram of the ion source and its holder is shown in Fig. 3. The capillary tube provides the transition from the target box pressure of 10^{3} torr to the skimmer box pressure of 10^{-1} torr, while the large 25 cm diffusion pump further reduces the operating pressure beyond the skimmer orifice to 10^{-4} torr. The entrance aperture on the ion source

serves to separate this region from the internal ion source pressure of $\sim 10^{-1}$ torr. A 0.75 mm tantalum filament heats the surroundings and acts as an electron source for the arc discharge maintained between the anode cap (Ta) and the hollow cathode tubes (Ta). Extraction and acceleration of a beam occurs via the 10.5 kV potential between the plasma and the grounded steel extractor. Steel was chosen for the extractor as well as the ion source housing in an attempt to utilize the large solenoid (crossed area in Fig. 3) as a focusing element for the beam as it is being extracted. The extracted beam immediately passes through the Einzel lens which is used to focus the beam into the rest of the optics system.

Normal operating conditions for the hollow cathode ion source consist of a helium supported arc heated by 330 ± 30 W of arc power and 200 ± 20 VA of filament power as applied to the 0.75 mm tantalum filament. Its holdup time is ~5 ms at a typical operating temperature of 1800°C.[35] The properties of this ion source have been investigated extensively both with internally produced (off-line) beams and with radioactivity generated by cyclotron bombardments. For certain cases, such as on-line tests with the rare-earth alpha-particle emitter ^{151}Dy (melting point = 1407°C), it appeared that the temperature of the plasma surroundings needed to be significantly above the melting point of the radioactive species, especially when the vapor pressure of an element is very low at its melting point. Extraction of these dysprosium ions, for example, only became possible when the filament power was raised to 300 VA. However, the discussion

below centers on results determined at the lower filament power (and an extraction potential of 10.5 kV).

Many additional properties of this ion source were defined by tests on the very stable plasma which exists under the arc parameters quoted above. The extracted ion current density is typically 300 mA/cm^2 of He^{+1}. Two tests were performed which demonstrated that, with a helium arc, almost total dissociation of most molecules occurs, with ionization confined primarily to the +1 charge state. First, tests with argon introduced as a very small impurity in the helium support gas produced a ratio for $^{40}Ar^{+1}/^{40}Ar^{+2} \approx 100$. Second, tests with oxygen under similar conditions produced a O^+/O_2^+ ratio of ~1000. Several further on-line tests with radioactivity using argon and neon as arc support gases indicated that the charge exchange reaction $He^+ + A \rightarrow A^+ + He$ is the predominant mode of ionization.

Surface ionization properties of the ion source must also be considered. It was mentioned above that the plasma surroundings must be maintained at a temperature significantly above the melting point of the species to be ionized. If not, the surroundings behave as a cold-finger vacuum pump and tend to trap the atoms of interest. Once trapped, any activity which ionizes on the cathode surfaces and is subsequently ejected with a positive charge cannot be accelerated into the plasma which is very near the anode potential. On the other hand, activity which leaves the anode cap with a positive charge can, return to the plasma for extraction. This surface ionization

phenomenon is indeed observed with the very volatile and easily ionized alkali metals and will be discussed in greater detail in the following paper.[27]

Coupling of an ion source to a beam transport system is necessarily dependent upon the properties of the plasma and the extracted beam characteristics. The latter is best characterized by the emittance which, when measured for this source at the 50% intensity level, was found to be 120 mm-mrad for $^{4}He^{+1}$ at 10.5 keV. This emittance was obtained by using a traditional slotted plate technique with a scanning wire arrangement discussed in more detail below.

The plasma conditions are determined primarily by four parameters: temperature (T_n) and density (ρ_n) of the neutral atoms, ion density (ρ_i), and electron temperature (T_e).[35] The efficiency of an ion source, defined as the ratio (R) of atoms ionized compared to the number introduced, is given in terms of the above parameters as

$$R = \left[1 + \frac{\rho_n}{\rho_i}\sqrt{\frac{T_n}{T_e}}\right]^{-1} . \qquad (2)$$

Equation (2) shows that for a particular type of ion source, the temperature of the electrons and the ion density need to be kept as high as possible. The electron temperature is governed by the arc voltage (~230 Volts) while the ion density is primarily governed by the electron density (for a given density of neutral atoms). The filament is the primary electron source and, therefore, the choice of

material is important. Originally filaments were constructed from 0.75 mm tantalum wire, which lasted ~85 hrs at 200 VA (but which evaporated rather quickly (~8 hrs) at filament powers of 300 VA). Improved results were obtained with filaments constructed from either 0.50 mm or 0.75 mm tungsten. The tungsten filaments have been found to give operating times of ~200 hrs at 200 VA (and ~50 hrs at 300 VA). To improve the overall reliability of this ion source, the tantalum cathode and anode pieces have been converted to molybdenum. Molybdenum was chosen because of its greater structural strength and its nearly identical coefficient of thermal expansion to that of tungsten.

The plasma is strongly affected by the solenoidal magnetic field created by the current passing through the filament. This field is significant (100-150 gauss) and does not permit the operation of the source with helium as a support gas when the magnetic field is mono-directional (DC filament supply) and unsuppressed. Although the addition of an external solenoid can make the effective field in the plasma region zero, our solution has been even simpler. We use an AC filament supply (60 Hz). This effectively extends the lifetime of electrons in the plasma which increases the electron density, and thereby increases the efficiency. No resolution degradation is noted due to this type of operation. Changes in the arc conditions change the observed resolution minimally while changing the magnetic field due to the filament dramatically affects the resolution.

The ions are extracted from the ion source and accelerated to their final energy of 10.5 keV by a simple conical grounded extractor electrode placed at distances of 5-10 mm (variable). The extractor is constructed from structural steel because it was hoped to use the focusing solenoid shown in Fig. 3 to increase the amount of beam output of the ion source. Tests with this solenoid succeeded only in extinguishing the arc and thus it was never used in actual experiments. This ion source, as coupled to the rest of the mass separator, meets most of the criteria desired: a) chemical universality for elements with melting points below 2000°C; b) very stable plasma conditions for long periods of time (days); c) short hold-up times (<5ms). The major drawback of this hollow cathode ion source is the low yield of elements whose melting points exceed 2000°C. One method to improve this efficiency would be to increase the electron temperature and density.

The measured efficiency for the ion source of 0.1 - 0.2% taken together with the ~10% efficiency for the rest of the system in principle permits us to observe roughly 75% of all elements produced with cross sections from 0.1 mb to 50 mb depending upon whether one is observing discrete energy charged particle decays or doing beta or gamma spectroscopy. These cross section limits are derived by considering the efficiencies in Table 1 (discussed further below) in relation to typical counting rates necessary for different types of experiments. The number of observable elements is based on the relative number of volatile elements with melting points $\leq$2000°C.

2.3 Beam Transport

Several factors need to be considered in designing an appropriate beam transport system for low energy beams. In the context of the RAMA design, complications arise because of the large extracted He^{+1} currents (100-200 μA) which can give rise to detrimental space charge effects with 10.5 keV beams. To eliminate the huge helium beam current, a Wien filter (see Fig. 1) is employed. The Wien filter is tuned for the mass of interest while deflecting the $^{4}He^{+1}$ away from the rest of the optics system.

In order to maximize the beam through the Wien filter, the beam is focused by an Einzel lens (see Fig. 1) maintained at a potential only slightly less (typically 9.5 kV) than the extraction potential (10.5 kV). The Einzel lens voltage is critical in that it determines the spot size through the Wien filter and, thus, the ultimate resolution. Before entering the Wien filter, the beam passes through a drift tube. In this region stray helium beam collides with the tube walls which eject electrons that mingle with the beam and effectively reduce space charge blowup. A suitable tube size was determined by measuring the $^{40}Ar^{+1}$ beam focused through the Wien filter as a function of tube radius (these electrons are not transmitted through the Wien filter.).

Although the Wien filter magnetic field is relatively inhomogeneous with significant fringing fields, this does not cause a problem since it is operated at a constant magnetic field (while tuning the electric field). However, it was necessary to use an

indirect method to establish the effective magnetic field. This was accomplished by determining the electric field needed to center the mass of interest versus $m^{-1/2}$ for several different beams. The slope of a plot of these results gives the value of $B_{eff}\sqrt{2E}$, where E is the beam energy, so that electric field settings can easily be calculated for any mass. Another requirement observed in later tests showed that the helium deflection angle needed to be between 4^{o} and 12^{o}. The 12^{o} limit is required to keep the helium beam from striking the electric field plates of the Wien filter while the 4^{o} limit is required to keep the helium beam from entering the remainder of the transport system. The resolution is dramatically worsened if these limits are exceeded.

The rest of the transport system (Fig. 1) was designed around a desired mass resolution $M/\Delta M$ of 200, a normal focal plane, a mass range of ±10%, and a double focus on the focal plane. The beam at the center of the Wien filter is treated as the virtual source for the optics. Calculations for this beam transport system were performed using standard electromagnetic formalism.[36-39] The first order calculations employ an electrostatic quadrupole triplet system (whose first and third elements operate together) to match the ion source emittance to the acceptance of the dipole analyzing magnet. (At low energies magnetic and electrostatic quadrupoles work equally well, but an electrostatic quadrupole may be tuned independently of the ion mass, making it the preferred choice.) Because of the availability of a surplus cyclotron beam bending magnet, a 75.5^{o} separator was designed.

A solution to the ion optics was obtained which transmitted 50% of the ion source output (based on the measured emittance) to the focal plane at the desired resolution of $M/\Delta M \sim 200$. A central ray of the beam entering the dipole magnet is bent 75.5^{o} and traverses entrance and exit edge angles of $\beta_1 = \beta_2 = 11^{o}$. A double focus was obtained on the focal plane with a small magnification in the x (radial) direction ($M_x \sim 0.5$) and a larger magnification in the y (vertical) direction ($M_y \sim 1.2$). This value for M_y poses no problem so long as neither collector nor detector dimensions are exceeded. A dispersion of 1.62 m was also calculated.

Second order calculations showed that aberrations were non-negligible. The beam is cylindrically symmetric with a divergence of ~30 mrad in both the x and y dimensions. This cylindrical symmetry created a need for both an upstream sextupole (SXT 1) and an entrance edge sextupole (there is no exit edge sextupole) because a reduction of the aberrations in one dimension caused an equivalent increase in the other dimension for a single sextupole system (see Fig. 1). If we denote the properties of a ray entering the dipole magnet with the vector notation of (x, x', y, y') where x and y are displacements and x' and y' are divergences, then we may write the initial vector as (x_o, x_o', y_o, y_o'). Since in our case $x_o' >> x_o$ and $y_o' >> y_o$, the most important second order aberrations are represented by terms in which x_o' and y_o' appear. The upstream sextupole and the entrance edge sextupole serve to minimize the largest second order matrix elements, namely the coefficients of the $(x_o')^2$ and $(y_o')^2$ terms.

To minimize the effects of the fringing field from the dipole magnet and to ensure a well-defined entrance edge sextupole, field clamps were installed. Field maps of the dipole magnet were obtained by a standard computerized mapping procedure,[40] providing a determination of the effective field boundary which was then used as input for the final optics calculation. The field maps also showed that the homogeneity of the magnetic field was sufficient to make shimming unnecessary. The calculations also showed that the focal plane angle was rotated 61^{o} to the ion trajectories which was deemed to be inconveniently steep. A downstream sextupole (SXT 2) was therefore incorporated to rotate the focal plane normal to the beam (or z) direction.

Extensive measurements of the beam properties on the RAMA focal plane were performed with internally produced $^{40}Ar^{+}$ beams. Figure 4 presents data on these properties as various optical elements are activated. These scans were obtained on the focal plane with a simple scanning wire arrangement connected to an x-y recorder; the beam current was measured as a function of either horizontal or vertical distance. The resolution values are all quoted at FW.1M (full width at one-tenth maximum) and are calculated from the equation $\mathrm{Res}(M/\Delta M) = \frac{D}{2w}$ where D is the dispersion and w is the measured peak width at one-tenth maximum. The first curve in Fig. 4 shows that very little beam was obtained when no elements except the dipole magnet were operative. Turning on the quadrupole triplet and the Wien filter gave a large increase in transmitted beam and a resolution of

~90. When next the downstream sextupole was turned on (third scan in Fig. 4), the focal plane was rotated to become normal to the z-axis while virtually no effect on the resolution was noted. The fourth curve in Fig. 4 shows the dramatic improvement in resolution (to ~195) when the upstream sextupole was turned on. This overall measured resolution compares well with the calculated value of 190. Further tests showed that the actual dispersion was 1.64 m (calculated 1.62 m) for the central ray. This dispersion varied from 1.68 m on the high mass side to 1.60 m on the low mass side of the ±10% mass range of the focal plane.

For general on-line beam tuning, the scanning wire arrangement is not useful because its required microampere current levels are often inconveniently high and require special arc support gas mixtures. Therefore, a channeltron electron multiplier was installed on the center line of the focal plane to permit tuning of the optics at more realistic beams levels (say 0.1-50 kHz). Basically, the channeltron electron multiplier produces an electron cascade for each charged particle that strikes its detection cone, yielding a current gain of 10^5-10^7; this current pulse is then collected in a Faraday cup and measured by a picoammeter. This system allows us to tune RAMA with the ^{40}Ar gas impurity contained in the helium arc support gas and, to a lesser extent, with the ubiquitous ^{39}K. It also permits the introduction of heavier, less volatile elements at a sufficiently low level to avoid affecting the operation of the ion source. For example, tin can be introduced into the arc by passing the support gas

over the non-volatile liquid tetraethyl tin(IV) (BP ~182°C), thereby providing a unique isotopic signature. This technique is very useful for calibrating RAMA in situ after the system has been operating for some time without disturbing the existing setup.

2.4 Detection Systems

Initial considerations in the design of a detector station were to provide maximum versatility for the wide variety of experimental arrangements anticipated. A detector box with a large number of ports was fabricated, necessitating large pumping capacities to maintain the detector box base pressure of 1×10^{-6} torr. Because of the large helium leak associated with the ion source, the normal operating pressure is 3×10^{-6} torr.

To separate adjacent masses, a movable slit system was designed. The slit width may be continuously adjusted from 0-20 mm about a movable point in the x-direction of the 16 cm focal plane. Rolling collimators attached to the slit arms keep activity from other masses from reaching the detector systems. Although only one system is normally employed in the center position, a second independent system can be used for studying a second mass position. Once the radioactivity of interest passes through the slits, it is collected for decay studies. One method of collection consists of stopping activity on a thin (300 $\mu g/cm^2$) aluminized polycarbonate foil mounted directly in front of either a single solid state detector or a detector telescope mounted on a movable arm. The actual detector mounts are electrically isolated and may be thermoelectrically cooled to temperatures approaching -40°C.

The collection and detection method described above is not optimum for decays involving heavy charged particle production because of the large energy loss (50-500 keV) of protons and alphas as they pass through the collector foil and the resulting peak broadening. This problem is overcome with a flipper wheel system shown schematically along with an operational sequence in Fig. 5. The flipper wheel arrangement permits only previously collected activity to be viewed by the appropriate solid state detector system. Though the flipper wheel system is very fast, rotating and stopping in approximately 40 ms, its stopping is inherently violent, creating a situation whereby only 1000-2000 flips are obtainable before some sort of realignment becomes necessary. Thus, it is not readily adaptable for activities with half-lives below 30 s. More reliability could easily be achieved by increasing the rotation time.

3. Initial Tests with Radioactivity

Initial tests of the RAMA system were performed with the beta-delayed alpha particle emitter ^{20}Na, produced via the $^{24}Mg(p,\alpha n)$ reaction at 40 MeV, due to its easily identifiable alpha groups and its short half-life of 446 ms. These tests included checking all of the optics parameters relative to calculated values based on the higher beam current scans of $^{20}Ne^{+1}$. Further tests of the RAMA system were performed with the much heavier nuclide ^{211}At ($t_{1/2}$ = 7.2h). This alpha-particle emitter was produced via the $^{209}Bi(\alpha,2n)$ reaction at 27 MeV. A scan of the mass 211 region with data from the alpha-particle decays of ^{211}At and its daughter, ^{211}Po, is shown in Fig. 6. The measured resolution of 205 was consistent with the off-line mass scans, and indicated that RAMA could be operated on a stable basis for many hours.

After these initial studies were completed, several more comprehensive tests were desired for the RAMA system. The light N = 84,85 rare-earth alpha-particle emitters, copiously produced in (HI, xn) reactions, were chosen because of their relatively short half-lives and their easily identifiable alpha groups. In addition, the masses of a number of the shorter-lived (<1 min) rare-earth alpha-particle emitters had only been established by systematic relationships, without any absolute verification. Initially, the well-known ^{150}Dy and ^{151}Dy isotopes were observed, produced in $^{142}Nd(^{12}C,xn)^{154-x}Dy$ reactions at 78 MeV, as was $^{149}Tb^{g}$ produced in the $^{142}Nd(^{11}B,4n)$ reaction at 62 MeV and in the

$^{141}Pr(^{12}C,4n)$ reaction at 78 MeV. Then, the masses of many of the light short-lived N = 84,85 isotones were determined in a series of experiments involving bombardments of ^{140}Ce, ^{141}Pr, ^{142}Nd, and ^{144}Sm targets with ^{11}B, ^{12}C, ^{14}N, and ^{16}O beams at various energies. These targets were in the form of oxides and nitrates supported by either copper or nickel backing foils. A typical alpha-particle spectrum collected on the flipper wheel and measured with a large surface barrier detector is shown in Fig. 7 while Table II summarizes our results compared to the literature assignments.[41] These results confirmed the mass assignments of most of the short-lived rare-earth alpha-particle emitters between holmium and ytterbium. Such a confirmation has been independently made in recent work by Hagberg, et al.[7] at ISOLDE in which decay studies of mass separated samples of ytterbium were observed in addition to subsequent daughter decays. Figure 8 presents a spectrum which confirmed the masses of both the high-and low-spin isomers of ^{151}Ho.

A second experiment of interest was motivated by the assignment of a 19 s beta-delayed proton activity to $^{111}_{52}Te$ by Bogdanov et al.[42,43] and to ^{110}Te by Macfarlane and Siivola.[44] Both of these assignments were initially based solely on excitation function and cross bombardment data. Figure 9 shows a proton spectrum obtained at the mass 111 position which coincides with that previously observed for this 19 s activity, clearly assigning it to the decay of ^{111}Te; this result has been separately confirmed by work reported from UNILAC.[8,9] Further studies in this region have led to our

observation of delayed protons from ^{109}Te and ^{112}I produced by the ^{102}Pd(^{12}C,5n) and ^{102}Pd(^{14}N,4n) reactions, respectively; these results agree with similar data reported by Kirchner, et al.[8] The study of these various elements with vastly different chemical properties and half-lives demonstrates the versatility of RAMA. A summary of the overall observed efficiencies for four of the activities mentioned above broken down in terms of their transmission through the various components of the RAMA system may be found in Table I.

4. Conclusions

The experiments discussed above have observed beams or activities of He^+, C^+, N^+, O^+, Ne^+, Na^+, Ar^+, K^+, Kr^+, Sn^+, Te^+, I^+, Xe^+, Tb^+, Dy^+, Ho^+, Er^+, Tm^+, Yb^+, and At^+, demonstrating the chemical versatility of a helium-jet fed, on-line mass analysis system such as RAMA. This list should readily be expandable with present techniques to ~75 of the known elements and with higher temperature ion sources to ~90 elements. RAMA is also a fast system, with the nominal helium-jet hold-up time of 200 ms being the only major time delay (species with half-lives as short as 400 ms have been experimentally observed). Substantial improvements to the RAMA system will be presented in the following paper.[27] The general capabilities of the RAMA system presented herein permit decay studies of many heretofore inaccessible nuclides.

5. Acknowledgements

We wish to thank the crew and staff of the 88-inch cyclotron for their aid and support during the construction and initial testing of the RAMA system. We also wish to thank D. Littlejohn for early groundwork and J. Wouters and R. Parry for their assistance during later tests of RAMA. In addition, we wish to thank R. Burton, D. Morris, and L. Glasgow for excellent engineering designs, and F. Selph, K. Halbach, R. Yourd, and J. Singh for their help in designing the optics system. Finally, we especially wish to thank Dr. D. Hendrie for advice on charged-particle transport systems and to D. Nelson for measurements of the dipole magnetic field.

References

1. K. L. Kosanke, W. C. McHarris, and R. A. Warner, Nucl. Instr. Meth. 115 (1974) 151.
2. K. Bächmann, V. Matschoß, J. Rudolf, A. Steffen, and S. Tsalas, Nucl. Instr. Meth. 139 (1976) 343.
3. J. P. Zirnheld, L. Schutz, and F. K. Wohn, Nucl. Instr. and Meth. 158 (1979) 409.
4. F. K. Wohn, in Proceedings of the Isotope Separator On-Line Workshop, R. E. Chrien, editor, Brookhaven National Laboratory, Upton, N. Y., Oct. 31-Nov. 1, 1977, BNL 50847, p. 23.
5. J. C. Hardy, Proc. Brookhaven (1977), BNL 50847, p. 309.
6. C. Detraz, D. Guillemand, G. Huber, R. Klapisch, M. Langevin, F. Naulin, C. Thibault, L. C. Carraz, and F. Touchard, Phys. Rev. C19 (1979) 164.
7. E. Hagberg, P. G. Hansen, J. C. Hardy, P. Hornshoj, B. Johnson, S. Mattson, and P. Tidemand-Peterson, Nucl. Phys. A293 (1977) 1.
8. R. Kirchner, O. Klepper, G. Nyman, W. Reisdorf, E. Roeckl, G. Schardt, N. Kaffrell, P. Peuser, and K. Schneeweiss, Phys. Lett. 70B (1977) 150.
9. E. Roeckl, R. Kirchner, O. Klepper, G. Nyman, and W. Reisdorf, Proc. Brookhaven (1977), BNL 50847, p. 331.
10. E. Spejewski, Proc. Brookhaven (1977), BNL 50847, p. 149.
11. R. G. H. Robertson, T. J. Bowles, and S. J. Freedman, Nucl. Instr. Meth. 147 (1977) 361.

12. V. A. Karnaukhov, D. D. Bogdanov, A. V. Demyanov, G. I. Koval, and L. A. Petrov, Nucl. Instr. Meth. 120 (1974) 69.

13. E. P. Wigner, Proceedings of the Robert A. Welch Conferences on Chemical Research, Houston, Texas, November 20-22, 1957, Vol. 1, p. 67.

14. W. Benenson and E. Kashy, to be published in Rev. Mod. Physics, MSUCL-278 (1979).

15. P. G. Hansen, to be published in Ann. Rev. of Nucl. and Part. Sci., CERN EP/79-11 (1979).

16. R. D. Macfarlane, R. A. Gough, N. S. Oakey, and D. F. Torgerson, Nucl. Instr. Meth. 73 (1969) 285.

17. J. M. Nitschke, in Proceedings of the International Conference on the Properties of Nuclei Far from the Region of Beta-Stability, Leysin, Switzerland, 1970 (CERN, Geneva, 1970) Vol. 1, p. 153.

18. J. Äystö, P. Puumalainen, and K. Valli, Nucl. Instr. Meth. 115 (1974) 65.

19. K. Wien, Y. Fares, and R. D. Macfarlane, Nucl. Instr. Meth. 103 (1972) 181.

20. H. Wollnik, J. Porstendörfer, R. Robig, and H. G. Wilheim, Nucl. Instr. Meth. 144 (1977) 247.

21. W. J. Wiesehahn, J. M. D'Auria, and J. C. Irwin, Nucl. Instr. Meth. 114 (1974) 401.

22. H. Jungclas, R. D. Macfarlane, and Y. Fares, Phys. Rev. Lett. 27 (1971) 556.

23. H. G. Wilhelm, H. Jungclas, H. Wollnik, D. F. Snider, R. Brandt, K. H. Lust, Nucl. Instr. Meth. 115 (1973) 419.

24. R. A. Gough, R. G. Sextro, and J. Cerny, Nuclear Chemistry Division Annual Report for 1972, LBL-1666, p. 361 (unpublished).

25. R. G. Sextro, Lawrence Berkeley Laboratory Report LBL-2360, Ph.D. Thesis, unpublished (1973).

26. HAVAR is a trade name for an alloy consisting primarily of Co (42.5%), Ni (13.0%), Cr (20.0%), and Fe (17.9%), with a density of 8.3 g/cm^3, and manufactured by the Metals Division of the Hamilton Watch Co., Lancaster, Pa.

27. D. M. Moltz, J. M. Wouters, J. Aysto, M. D. Cable, R. F. Parry, R. D. von Dincklage, and Joseph Cerny, Report No. LBL-9721, Nucl. Instr. Meth., the following paper.

28. J. B. Anderson, R. P. Andres, and J. B. Fenn, Advan. Chem. Phys. 10 (1966) 275.

29. J. P. Zirnheld, Nucl. Instr. Meth 120 (1974) 1.

30. H. Schmeing, V. Koslowsky, M. Wightman, J. C. Hardy, J. A. MacDonald, F. Faestermann, H. R. Andrews, J. S. Geiger, and R. L. Graham, Nucl. Instr. Meth. 139 (1976) 335.

31. G. Sidenius, Nucl. Instr. Meth. 151 (1978) 349.

32. R. Kirchner and E. Roeckl, Nucl. Instr. Meth. 131 (1975) 371.

33. R. Kirchner and E. Roeckl, Nucl. Instr. Meth. 133 (1976) 187.

34. R. Kirchner and E. Roeckl, Nucl. Instr. Meth. 139 (1976) 291.

35. G. Sidenius, in Proceedings of the First International Conference on Ion Sources, Saclay, France (1969) p. 401.

36. All optics calculations were performed using standard beam transport equations contained in the codes BELIN (first order) and DESS (second order) provided by Frank Selph.

37. A. P. Banford, in The Transport of Charged Particle Beams, E. & F. N. Spon, Ltd. (1966) p. 1.

38. E. Regenstreif, in Focusing of Charged Particles, A. Septier, editor, Academic Press (1967) Vol. 1, p. 353.

39. D. L. Hendrie, in Nuclear Spectroscopy and Reactions, J. Cerny, editor, Academic Press (1974) Part A, p. 365.

40. C. G. Dols, in 4th International Conference on Magnet Technology, Y. Winterbottom, editor, Brookhaven National Laboratory, Upton, N. Y., Sept. 19-22, 1972, p. 791.

41. H. Gauvin, Y. LeBayec, J. Livet, and J. L. Reyss, Ann. Phys. 9 (1975) 241.

42. D. D. Bogdanov, I. Bacho, V. A. Karnaukhov, and L. A. Petrov, Sov. J. Nucl. Phys. 6 (1968) 650.

43. D. D. Bogdanov, I. Bacho, V. A. Karnaukhov, and L. A. Petrov, Sov. J. Nucl. Phys. 6 (1968) 807.

44. R. D. Macfarlane and A. T. Siivola, Phys. Rev. Lett. 14 (1964) 114.

Figure Captions

Fig. 1. Overall schematic diagram of RAMA.

Fig. 2. Photograph of the RAMA helium-jet box. The target would normally be directly in front of the collection cyclinder.

Fig. 3. Schematic diagram of the RAMA ion source region.

Fig. 4. Effects of various ion optical devices on an $^{40}Ar^{+1}$ beam as horizontally scanned on the RAMA focal plane. See text.

Fig. 5. Schematic diagram of the flipper wheel system. The sequence of events corresponding to a single 180^{o} rotation is listed.

Fig. 6. Scan of mass 211 using the alpha-particle emitter ^{211}At produced by the $^{209}Bi(\alpha,2n)$ reaction at 27 MeV.

Fig. 7. ^{153}Er alpha-particle spectrum at the mass 153 position on the RAMA focal plane; this isotope was produced by the $^{142}Nd(^{16}O,5n)$ reaction.

Fig. 8. An alpha-particle spectrum at the mass 151 position resulting from decay of ^{151}Ho isomers produced by ^{14}N-induced reactions on ^{142}Nd at 90 MeV bombarding energy.

Fig. 9. Proton spectrum at the mass 111 position from ^{111}Te produced by the $^{102}Pd(^{12}C,3n)$ reaction at 70 MeV.

Table I. RAMA efficiencies

	^{20}Na	^{111}Te	^{150}Dy	^{211}At
He-jet	20%[a]	60%	10%[a]	15%[a]
Skimmer	70%	60%	60%	70%
Ion Source	0.2_3%	0.1_2%	~0.2%	0.2%
Magnetic Analysis[b]	50%	50%	50%	50%
Overall	0.016%	0.02%	0.01%	0.01%

a) Not optimized.

b) Calculated based on measured ion source emittance.

Table II. Rare-earth alpha-particle emitter mass confirmations.

Nuclide	Z	Alpha Particle Decay Energies (MeV)		$t_{1/2}$	
		Observed[a]	Literature[b]	Observed	Literature[b]
$^{149}Tb^{g}$	65	3.95	3.95	4.07 ± 1.0 h	4.1 ± 0.2h
^{151}Dy	66	4.07	4.07	17.5 ± 0.5 m	17.7 ± 0.5m
^{150}Dy	66	4.23	4.23	7.1 ± 0.7 m	7.2 ± 0.1m
^{152}Ho(High Spin)	67	4.45	4.46	53 ± 4s	52.3 ± 0.5s
^{152}Ho(Low Spin)	67	4.38	4.38	2.0 ± 0.5 m	2.36 ± 0.4m
^{151}Ho(High Spin)	67	4.51	4.52	36 ± 2 s	35.6 ± 0.4s
^{151}Ho(Low Spin)	67	4.60	4.60	37 ± 8 s	42 ± 4s
^{153}Er	68	4.68	4.67	35 ± 2 s	36 ± 2s
^{152}Er	68	4.82	4.80	-	9.8 ± 0.3s
$^{154}Tm^{m}$	69	5.02	5.04	-	3.0 ± 0.2s
^{155}Yb	70	5.19	5.21	-	1.65 ± 0.15s
^{154}Yb	70	5.32	5.33	-	400 ± 4.0ms

a) Typical errors are ±0.03 MeV.

b) Ref. 41.

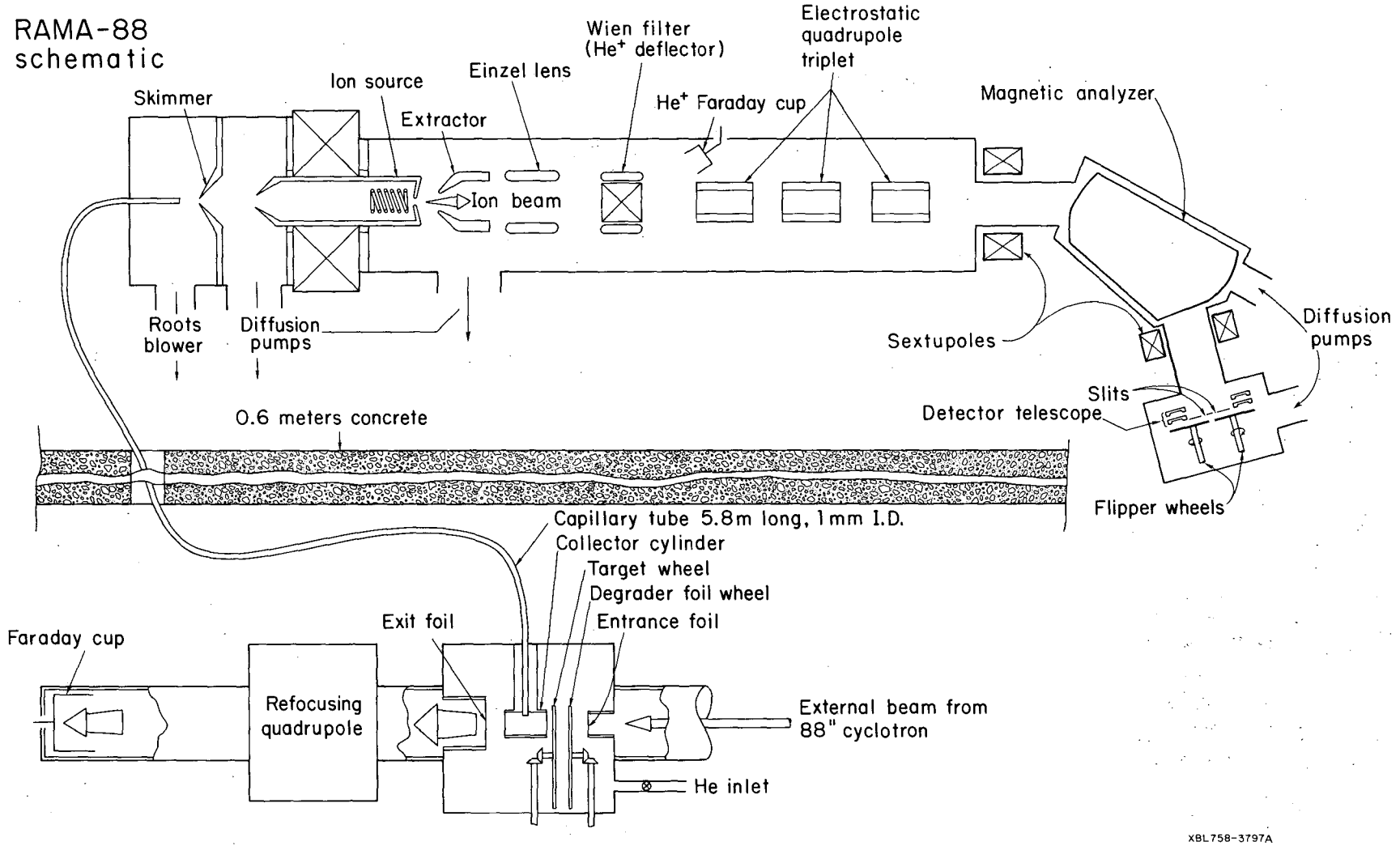
RAMA-88
schematic
Skimmer
Ion source
Extractor
Einzel lens
Wien filter
(He+ deflector)
He+ Faraday cup
Electrostatic
quadrupole
triplet
Magnetic analyzer
Ion beam
Roots
blower
Diffusion
pumps
Sextupoles
Diffusion
pumps
Slits
Detector telescope
0.6 meters concrete
Flipper wheels
Capillary tube 5.8m long, 1mm I.D.
Collector cylinder
Target wheel
Degrader foil wheel
Entrance foil
Exit foil
Faraday cup
Refocusing
quadrupole
External beam from
88" cyclotron
He inlet
XBL758-3797A

Fig. 1

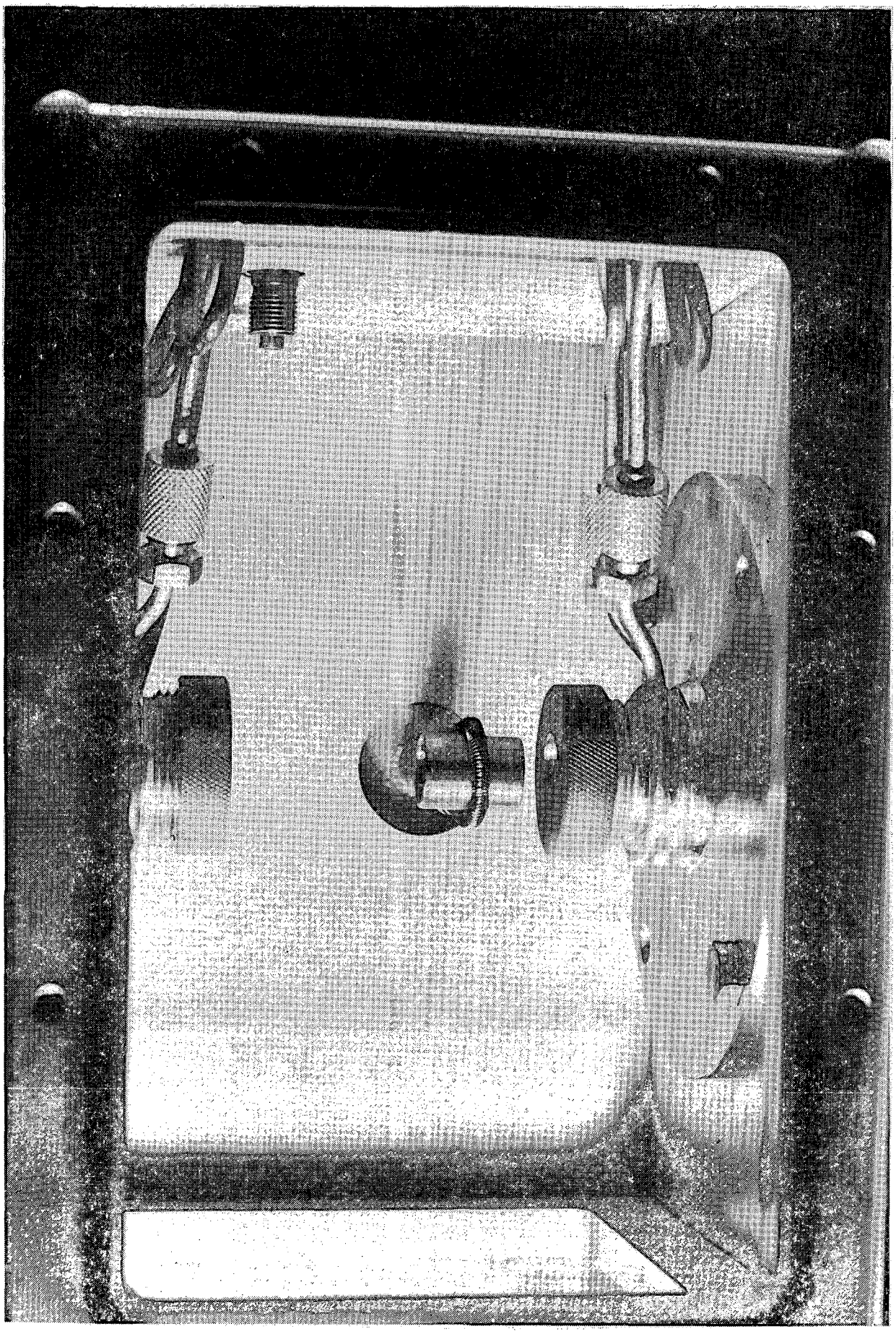

CBB 723-1572

Fig. 2

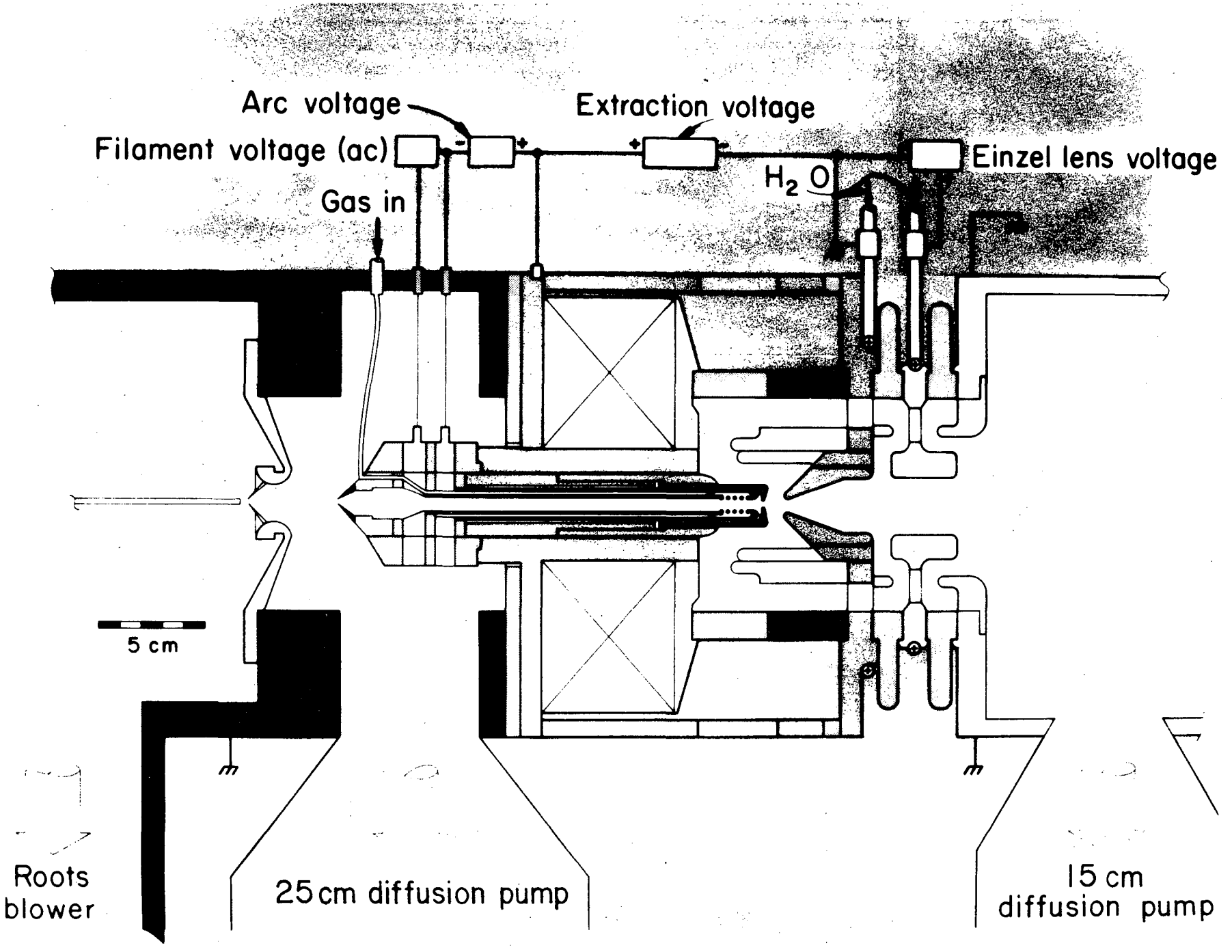
Arc voltage
Filament voltage (ac)
Gas in
Extraction voltage
H_2O
Einzel lens voltage
5 cm
Roots blower
25 cm diffusion pump
15 cm diffusion pump

Fig. 3

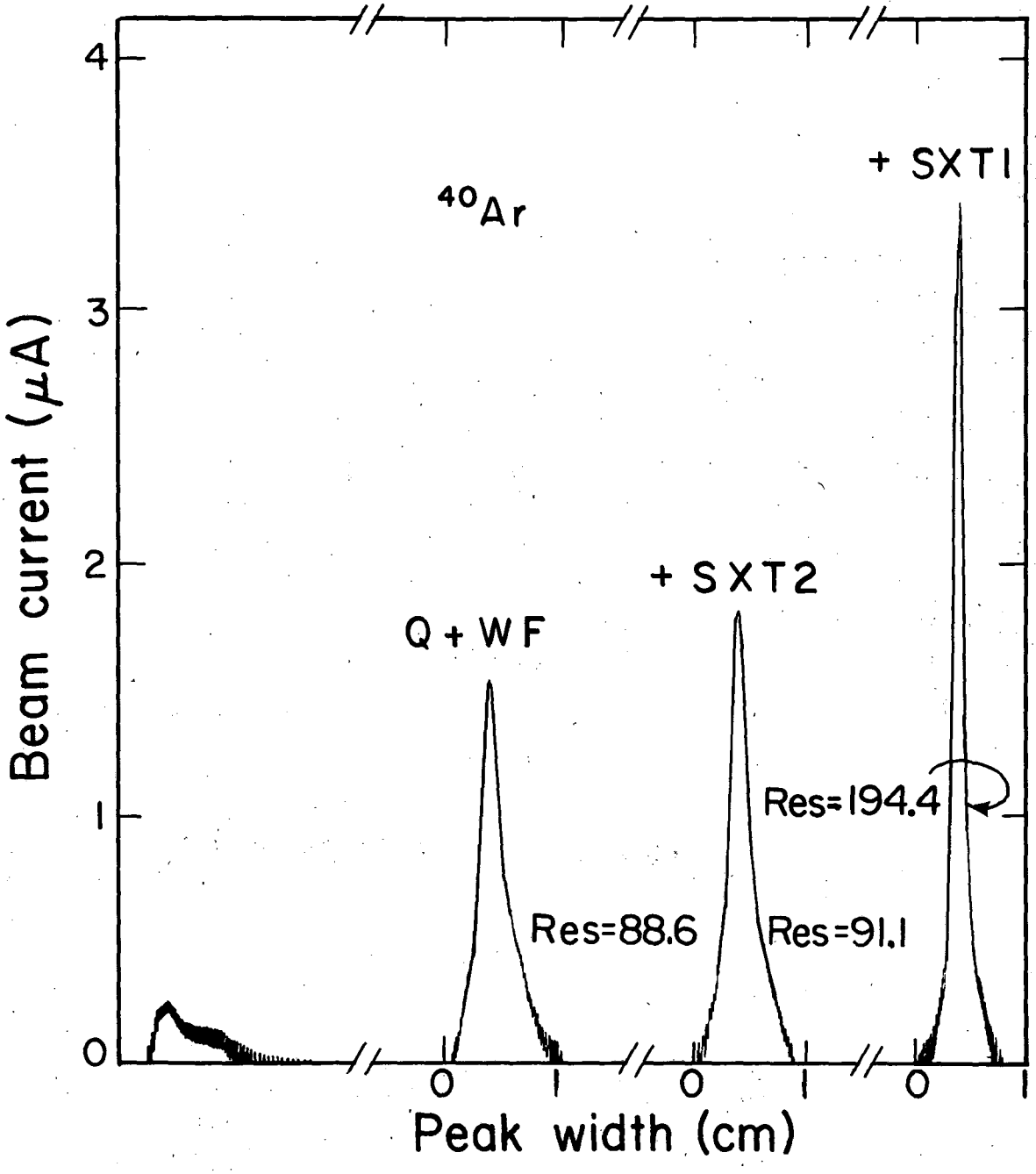

XBL 7612-4594

Fig. 4

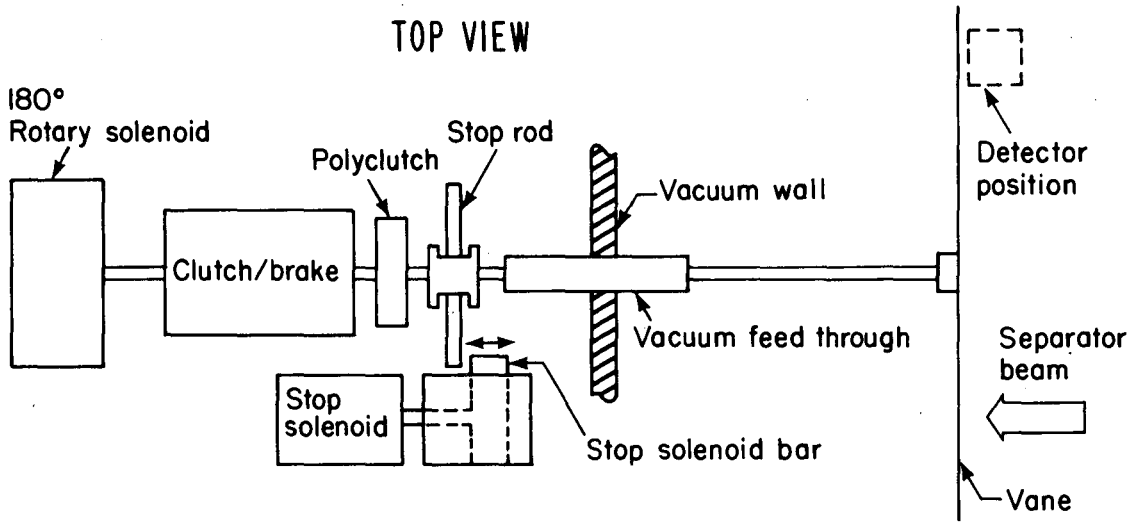

SEQUENCE OF EVENTS:

1) CLUTCH/BRAKE ENERGIZED TO CONNECT ROTARY SOLENOID TO SHAFT.

2) ROTARY SOLENOID ACTUATED ROTATING SHAFT 180°.

3) STOP SOLENOID ENERGIZED AFTER SHAFT HAS ROTATED ~ 90° PULLING STOP IN PATH OF STOP ROD.

4) AFTER TRAVELLING 180°, CLUTCH/BRAKE DE-ENERGIZES STOPPING ROTATION AND ALLOWING ROTARY SOLENOID TO RELAX.

5) STOP ROD HITS STOP SOLENOID BAR AFTER TRAVELLING EXACTLY 180°.

6) STOP SOLENOID RELAXES.

7) POLYCLUTCH ALLOWS ROTATION ONLY IN ONE DIRECTION PREVENTING BACK-SPIN WHEN STOP ROD HITS STOP SOLENOID BAR.

Fig. 5

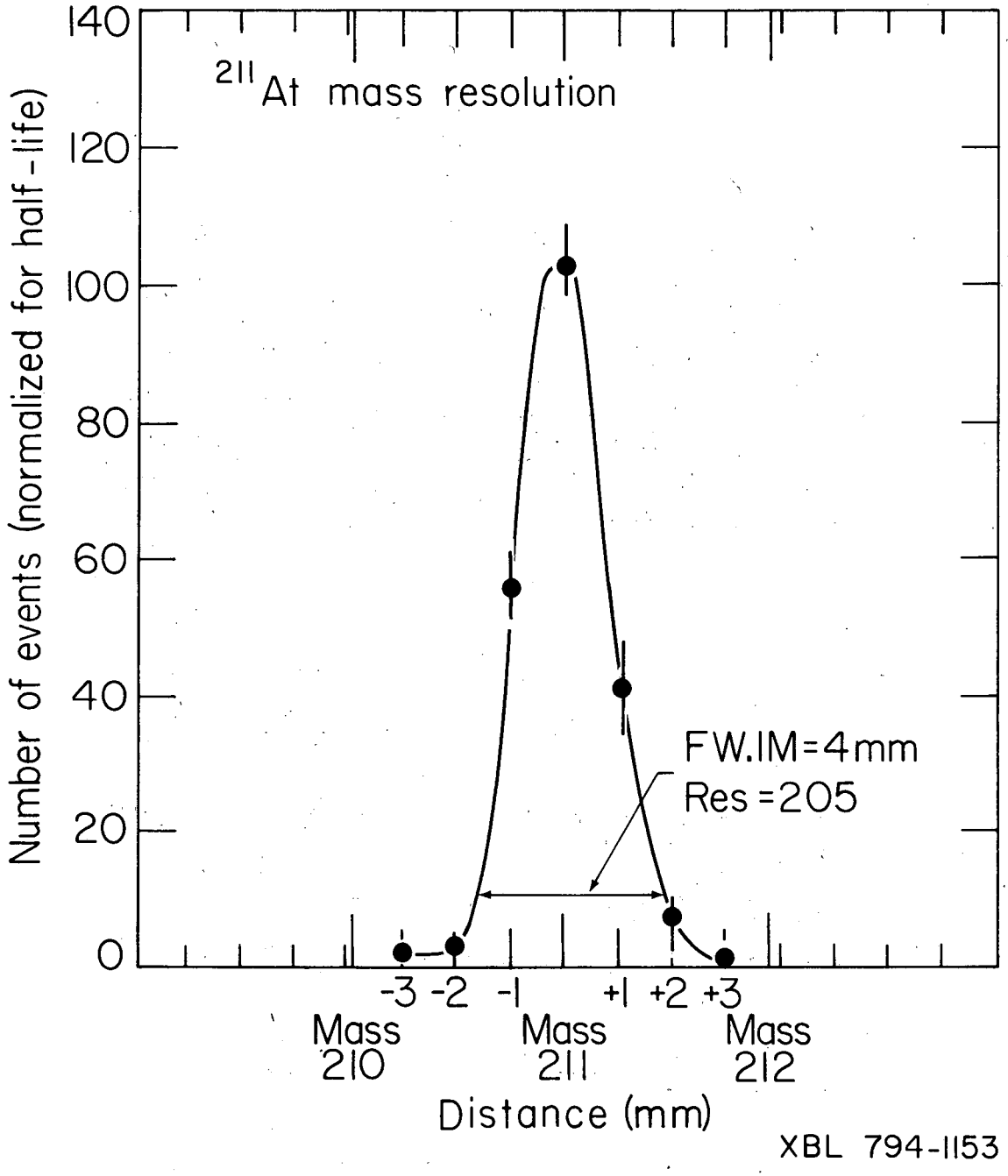
^{211}At mass resolution
Number of events (normalized for half-life)
140
120
100
80
60
40
20
0
FW.IM=4mm
Res =205
-3 -2 -1 +1 +2 +3
Mass 210
Mass 211
Mass 212
Distance (mm)
XBL 794-1153

Fig. 6

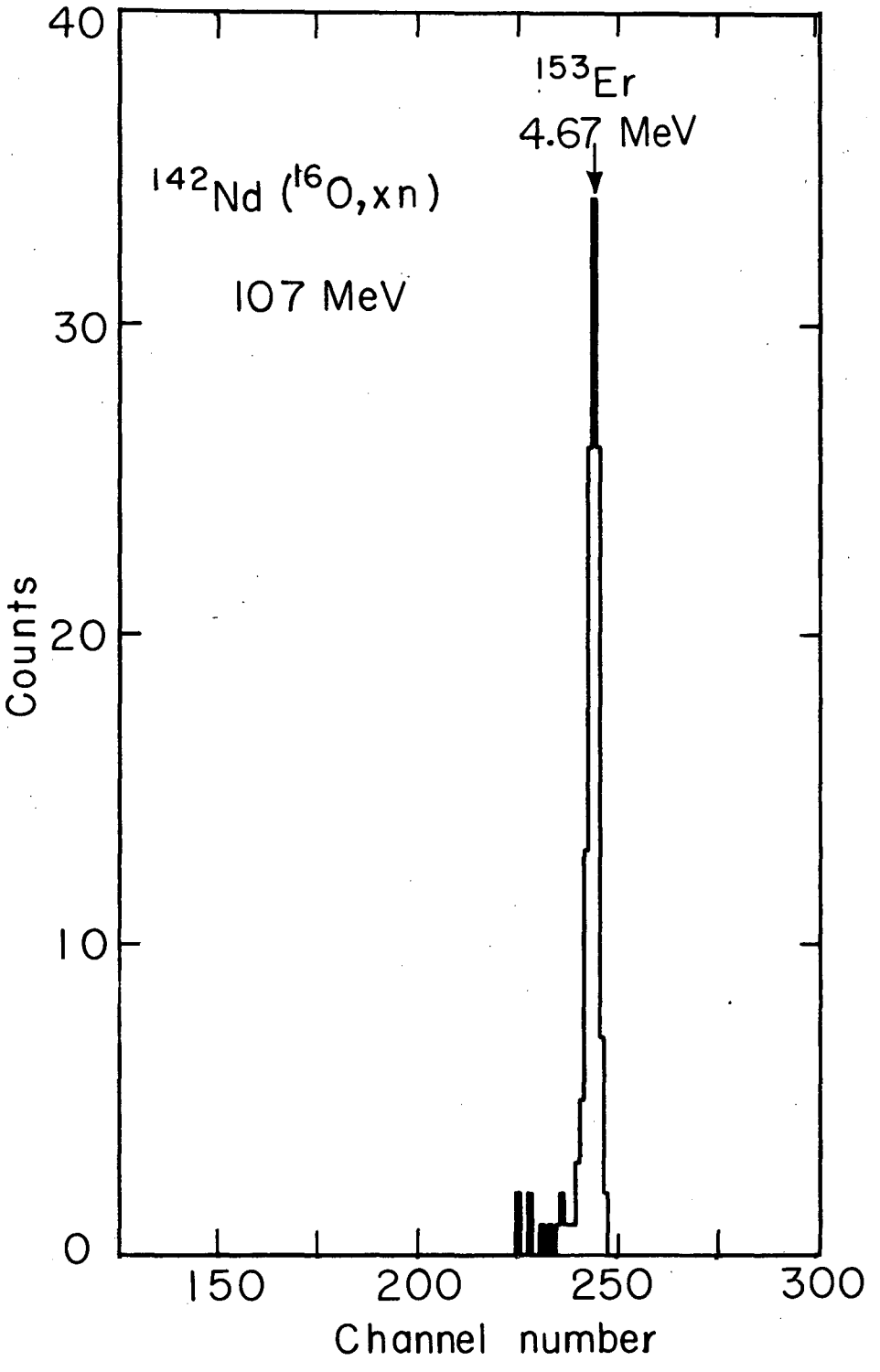

Fig. 7 XBL776-1484

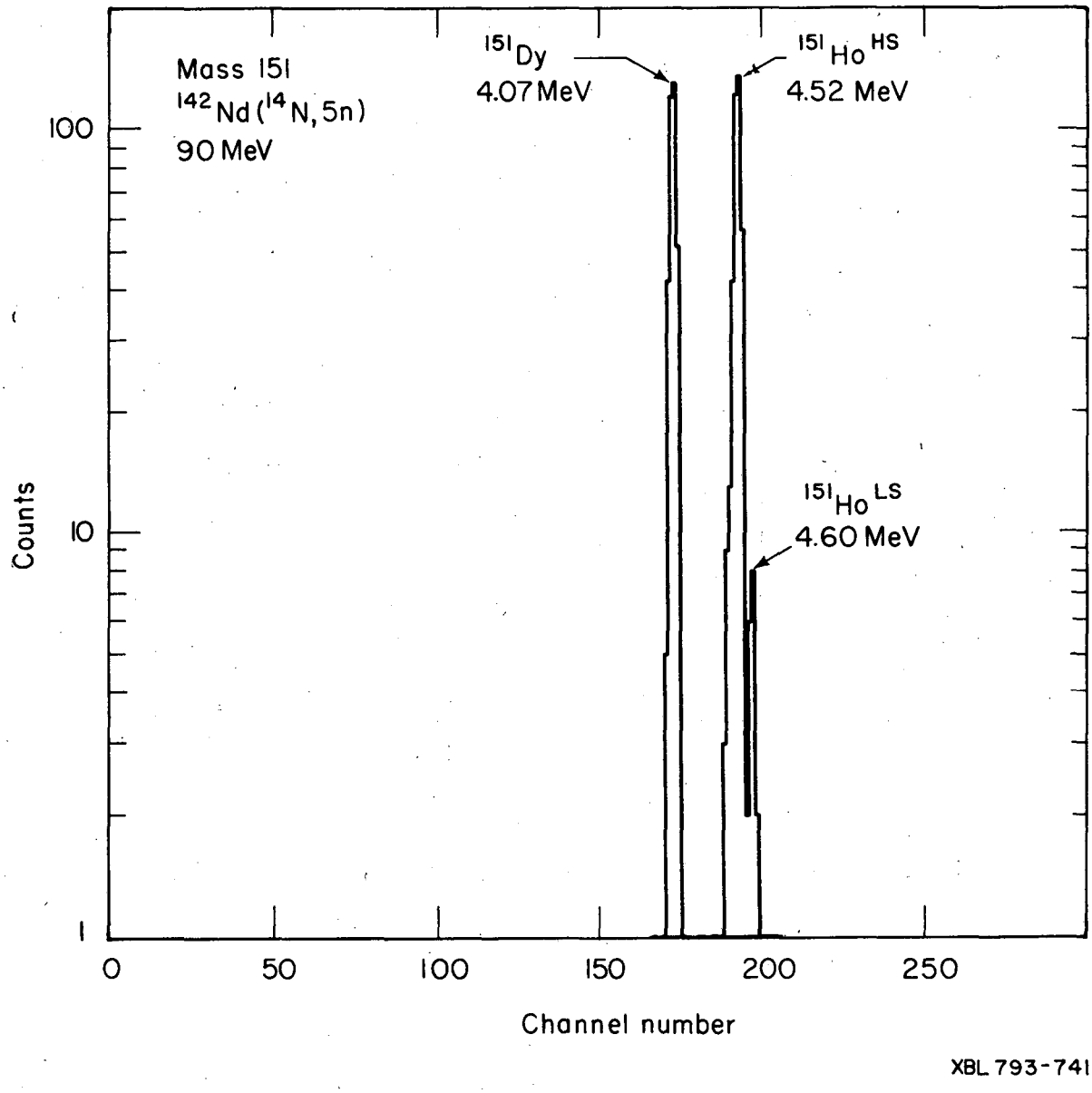
Mass 151
142Nd(14N,5n)
90 MeV
151Dy
4.07 MeV
151Ho HS
4.52 MeV
151Ho LS
4.60 MeV
Counts
100
10
1
0
50
100
150
200
250
Channel number
XBL 793-741

Fig. 8

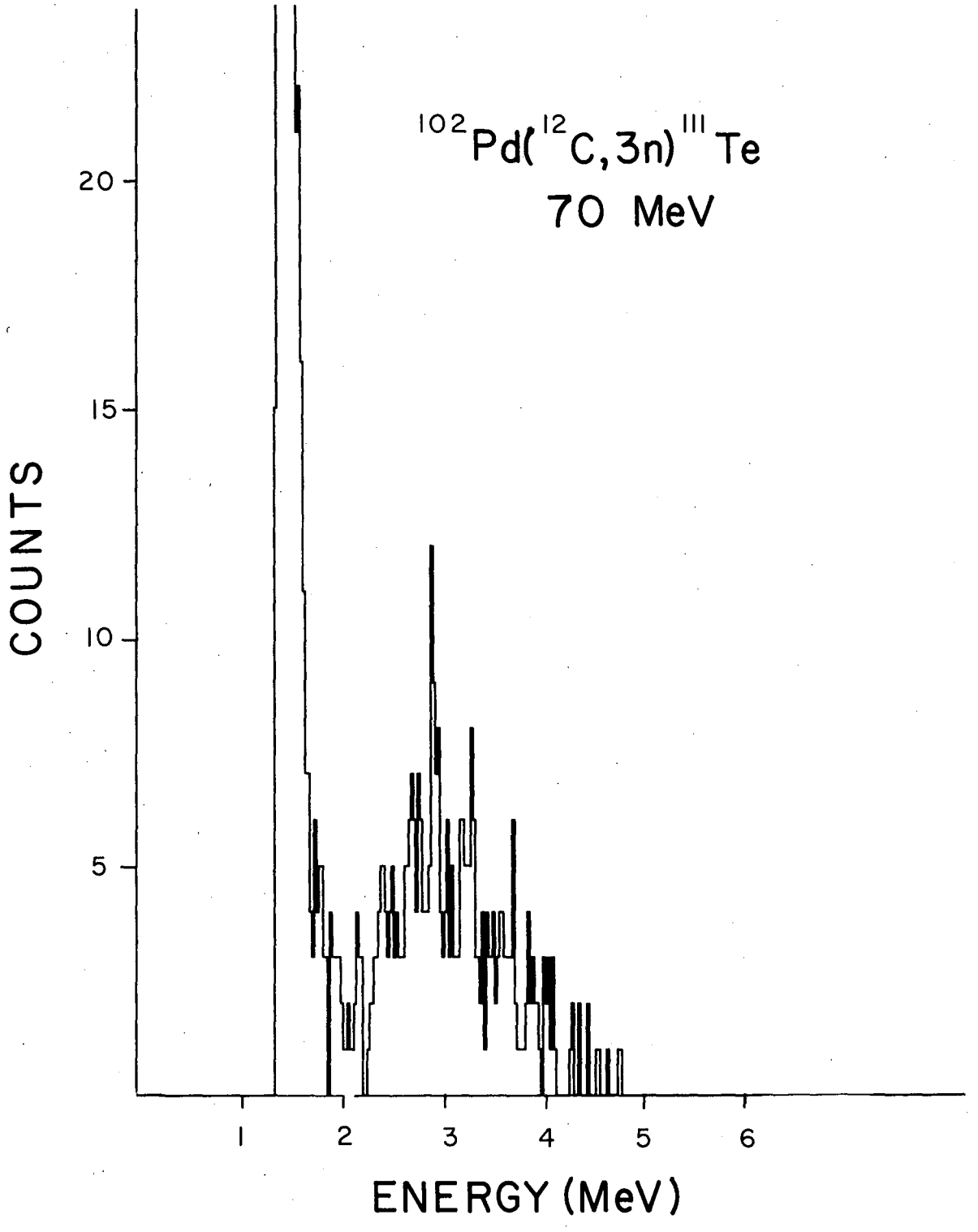

Fig. 9

XBL 7711-10433

TECHNICAL INFORMATION DEPARTMENT
LAWRENCE BERKELEY LABORATORY
UNIVERSITY OF CALIFORNIA
BERKELEY, CALIFORNIA 94720